Gastric carcinoma harbouring loss-of-function mutations in the *PIK3R1*, *ATRX* and *RBM10* genes exhibits diverse histological features associated with EBV infection and *TP53* inactivation: A case report

SE UN JEONG[1], EUNO CHOI[2], YONGIL KIM[3], JAEYOUNG BYEON[4] and SO-WOON KIM[1]

[1]Department of Pathology, Kyung Hee University Hospital, Kyung Hee University College of Medicine, Seoul 02447, Republic of Korea; [2]Department of Pathology, Ewha Woman's University Mokdong Hospital, Ewha Woman's University College of Medicine, Seoul 07985, Republic of Korea; [3]Department of Surgery, Ewha Woman's University Mokdong Hospital, Ewha Woman's University College of Medicine, Seoul 07985, Republic of Korea; [4]LabGenomics Clinical Research Institute, LabGenomics, Seongnam, Gyeonggi 13488, Republic of Korea;

Received July 25, 2024; Accepted February 5, 2025

DOI: 10.3892/ol.2025.15002

Abstract. This study presents a novel case of gastric carcinoma (GC) with diverse histological features and unique molecular alterations. A 62-year-old man with hematemesis was diagnosed with advanced GC and hepatic metastasis. Despite palliative gastrectomy to control bleeding, the patient succumbed within 6 months. Histological examination revealed three distinct tumour components: Gastric adenosquamous carcinoma (GASC), GC with lymphoid stroma (GCLS) and poorly differentiated adenocarcinoma (PDAD). Immunohistochemical staining, next-generation sequencing and Epstein-Barr virus (EBV) *in situ* hybridisation were performed to characterise the tumour. The GASC component revealed diffuse p40 and p63 immunoreactivity, while the GCLS and PDAD components were negative for both markers. All components harboured a missense mutation in the phosphoinositide-3-kinase regulatory subunit 1 gene and deletions in the *ATRX* and RNA binding motif protein 10 genes. Additionally, the GCLS component was EBV positive and the PDAD component demonstrated concurrent EBV infection and *TP53* inactivation. The present case highlights the importance of thorough molecular and histological evaluation, as distinct molecular alterations and heterogenous EBV status in histologically diverse components may significantly influence patient prognosis and treatment strategies.

Correspondence to: Dr So-Woon Kim, Department of Pathology, Kyung Hee University Hospital, Kyung Hee University College of Medicine, 23 Kyungheedae-ro, Dongdaemun, Seoul 02447, Republic of Korea
E-mail: swkdek@gmail.com

Key words: Epstein-Barr virus, phosphoinositide-3-kinase regulatory subunit 1, ATRX, RNA binding motif protein 10, stomach neoplasm, *TP53*

Introduction

Gastric carcinoma (GC) is one of the most prevalent cancers worldwide, ranking fifth in incidence and fourth in cancer-related mortality globally (1). Risk factors for GC include *Helicobacter pylori* infection, dietary habits, smoking and genetic predispositions (2). Despite advancements in surgical techniques, chemotherapy and targeted therapies, early diagnosis of GC remains challenging due to non-specific symptoms, often resulting in a poor prognosis at the advanced stages (3). Current challenges in GC management include the development of treatment resistance and the need for personalized therapeutic approaches (4). Phosphoinositide-3-kinase regulatory subunit 1 (PIK3R1) is a key regulatory subunit of phosphoinositide 3-kinases, acting as a tumor suppressor by inhibiting the activity of p110α of class I PI3K (PIK3CA) (5). Mutations in *PIK3R1* have been implicated in tumorigenesis across multiple organs (6), and elevated levels of PIK3R1 are associated with the progression of GC (7,8).

ATRX, a regulator of the chromatin state, gene expression, cellular senescence and DNA damage repair, belongs to the SWI/SNF protein family. Loss of *ATRX* expression is associated with activation of the alternative lengthening of telomeres pathway, contributing to the replicative immortality of cancer cells (9,10). Loss-of-function (LOF) mutations in *ATRX* are linked to aggressive traits such as tumour growth, migration, invasion and metastasis in osteosarcoma (9). Although the role of *ATRX* in GC is not well understood, female patients with GC harbouring *ATRX* mutations exhibit microsatellite instability-high subtypes, elevated tumour mutational burden and increased programmed cell death ligand-1 (PD-L1) expression. Moreover, those patients exhibit prolonged survival when treated with immune checkpoint inhibitors (11).

RNA binding motif protein 10 (RBM10), an alternative splicing factor protein, regulates RNA transcription and expression, including pre-mRNA splicing, mRNA stabilisation and mRNA transcription. *RBM10* is recognised as a tumour suppressor gene that inhibits proliferation, invasion

and metastasis while promoting apoptosis during tumorigenesis (12,13). However, *RBM10* has also been shown to promote cancer via a negative feedback mechanism, driven by the upregulation of *RBM10* or its homolog (13). As with *ATRX*, there have been few studies on *RBM10* in GC, but upregulation of *RBM10* has been confirmed in The Cancer Genome Atlas (TCGA) dataset (14).

Epstein-Barr virus (EBV) is an oncogenic virus that can contribute to the malignant transformation of normal gastric cells (15). The primary route by which EBV infects epithelial cells is through direct cell-to-cell contact mediated by B lymphocytes. Following persistent infection, EBV enters latency, during which it does not integrate into the host genome but replicates concurrently with the host cells (16). *EBV* exhibits a distinct gene expression profile depending on the latency type. EBV-positive GC (EBVpGC) is closely associated with latency type 1 genes, including EBV-encoded small RNA 1 (EBER1), EBER2 and EBV nuclear antigens 1 (16). EBVpGC is distinguished from other types of GC by its characteristic genomic aberrations, distinct clinicopathological features and generally favourable prognosis (17). In GC, *PIK3R1* mutations are associated with EBVpGC cases, whereas *TP53* inactivation is typically identified in EBV-negative GC (EBVnGC) cases (18).

In the present study, a GC case with a poor prognosis, harbouring LOF mutations in the *PIK3R1*, *ATRX* and *RBM10* genes, with diverse histological features associated with EBV infection and *TP53* inactivation is reported.

Case report

In April 2023, a 62-year-old man presented to the Emergency Department of Ewha Woman's University Mokdong Hospital (Seoul, Republic of Korea) with hematemesis. The patient's initial vital signs were stable. Although the patient had a history of infarction in the left middle cerebral artery and was receiving antithrombotic therapy (aspirin and clopidogrel), there was no history of cancer. Abdominal computed tomography revealed an encircling mass in the lower gastric body (Fig. 1A), multiple metastatic lymph nodes near the celiac axis and gastroepiploic vessels as well as peritoneal seeding, suggestive of unresectable advanced GC. Following admission, numerous well-defined lesions of varying sizes, highly suspected of representing hepatic metastasis, were identified in both hepatic lobes via diffusion-weighted magnetic resonance imaging (Fig. 1B). Esophagogastroduodenoscopy confirmed active bleeding from exposed vessels with detached blood clots (Fig. 1C). Given the active bleeding and the challenges of initiating chemotherapy immediately, palliative subtotal gastrectomy and liver excisional biopsy were selected as the initial intervention. Macroscopically, a well-defined, ulcero-infiltrative mass measuring 7.0x6.0x1.2 cm was identified on the posterior wall of the gastric body and antrum (Fig. 2A). The cut surface was greyish-white, solid and necrosis-free, with direct invasion into the serosa (Fig. 2B). For histological examination, the tissues were paraffin-embedded following fixation in 10% neutral-buffered formalin at room temperature (~25˚C) for 24 h. Sections were cut at a thickness of 4 μm and stained with haematoxylin for 5 min and eosin for 2 min at room temperature. The prepared slides were examined using a light microscope (Leica DM2000; Leica Microsystems, Inc.). Microscopically, the tumour consisted of three distinct histological components: Gastric adenosquamous carcinoma (GASC), GC with lymphoid stroma (GCLS) and poorly differentiated adenocarcinoma (PDAD), accounting for 30, 40 and 30% of the tumour volume, respectively. The GASC component comprised of both adenocarcinoma and squamous cell carcinoma, characterised by large round-to-oval nuclei with abundant eosinophilic cytoplasm, intercellular bridges and multifocal glandular formations (Fig. 3A). No keratin pearls were observed. This component was primarily located in the mucosal and submucosal layers. The GCLS component exhibited abundant lymphocytic infiltration around undifferentiated carcinoma clusters with lacy or tubular growth patterns, pleomorphic polygonal cells, prominent nucleoli and vesicular chromatin (Fig. 3B). The PDAD component featured relatively small, monotonous, hyperchromatic nuclei with coarse chromatin, prominent nucleoli and brisk mitotic activity. This component had a mucinous stromal background, with rare glandular formations and minimal lymphocytic infiltration (Fig. 3C). The GCLS and PDAD components were primarily located in the muscularis propria and subserosa.

To assess biomarker expression and the molecular characteristics of the three histological components, mucicarmine staining, immunohistochemical (IHC) analysis, EBV *in situ* hybridisation and next-generation sequencing (NGS) were conducted. For mucicarmine staining, the Artisan Mucicarmine Stain Kit (Agilent Technologies; cat. no. AR168) was used. The protocol involved deparaffinizing and hydrating sections, staining with Weigert's Iron haematoxylin for 10 min at room temperature, followed by incubation in Working Mucicarmine Solution for 30-60 min at room temperature. After washing, the sections were counterstained with Tartrazine Solution for 30 sec to 1 min at room temperature, then dehydrated, cleared and mounted. This method stains mucin in pink, nuclei in black and the background in yellow. For immunostaining, the tissues were paraffin-embedded and fixed in 10% neutral-buffered formalin at room temperature for 24 h. Sections were cut at a thickness of 4 μm and dried at 55˚C for 3 h. Heat-induced epitope retrieval was performed at pH 9.0 for 20 min using a Leica-Bond Autostainer and a Bond Polymer Refine Detection Kit (cat. no. DS9800; Leica Biosystems). Endogenous peroxidase activity was quenched using 3% hydrogen peroxide at room temperature for 10 min. Primary antibodies were incubated at room temperature for 1 h, with details of the antibodies and dilutions provided in Table SI. Secondary antibody incubation was performed using the aforementioned Bond Polymer Refine Detection Kit, and staining was visualized with diaminobenzidine (DAB) chromogen. The prepared slides were examined using a light microscope (Leica DM2000; Leica Microsystems, Inc.). p40 and p63 staining identified the squamous cell carcinoma component, while synaptophysin and chromogranin staining detected the neuroendocrine carcinoma component. To classify the molecular subtype according to the Asian Cancer Research Group, mutL homolog 1 (MLH1), mutS homolog 2 (MSH2), p53 and E-cadherin staining were performed (19). PD-L1 and programmed cell death protein-1 (PD-1) are known to be frequently upregulated, while human epidermal growth factor receptor 2 (HER2) typically shows negative expression in EBVpGC (20). EBV *in situ* hybridisation was

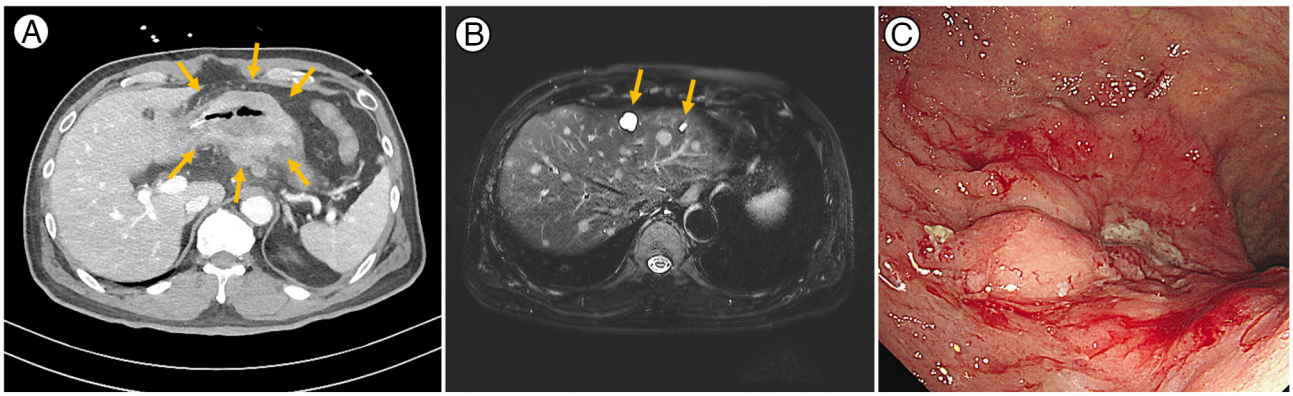


Figure 1. Images and endoscopic findings. (A) Abdominal computed tomography scan of a large encircling mass in the gastric lower body (arrows). (B) Diffusion-weighted magnetic resonance imaging of multiple lesions in both hepatic lobes (arrows). (C) Esophagogastroduodenoscopy image of a ulceroinfiltrative mass with bleeding focus.

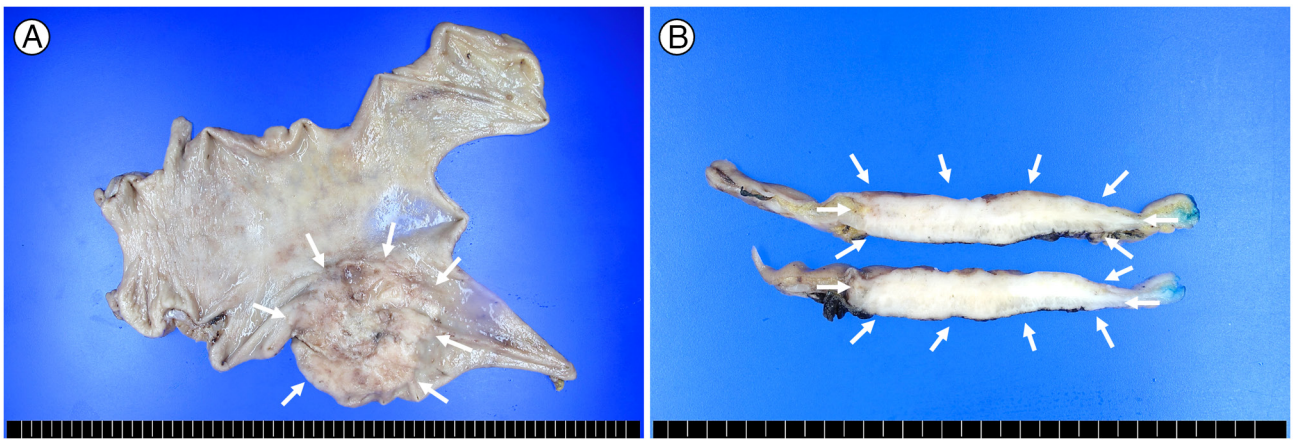


Figure 2. Macroscopic findings of the tumour. (A) A large, well-defined and ulceroinfiltrative mass (7.0x6.0x1.2 cm) as identified at the posterior wall of the lower body and antrum (arrows). (B) The tumour directly invaded the serosa (the area of the tumour is indicated by arrows).

performed to detect EBER RNA sequences in formalin-fixed, paraffin-embedded tissue sections. The tissues were fixed in 10% neutral-buffered formalin at room temperature for 24 h and embedded in paraffin. Sections were cut at a thickness of 4 μm and deparaffinized prior to hybridization, and permeabilized using proteinase K (cat. no. S3020; Dako; Agilent Technologies, Inc.) at 37˚C for 15 min. Hybridization was conducted using Bond hybridization buffer (cat. no. PB0589; Leica Biosystems) with the biotin-labelled Epstein-Barr Virus Early EBER RNA Probe (Invitrogen; Thermo Fisher Scientific, Inc.; cat. no. 551019) at a concentration of 0.5 μg/ml, incubated at 45˚C for 20-60 min. Post-hybridization washes were performed with saline-sodium citrate buffer at 45˚C to remove excess probes, followed by blocking endogenous peroxidase activity using 3% hydrogen peroxide at room temperature for 10 min. Detection was carried out using the Bond Polymer Refine Detection Kit (Leica Biosystems, Ltd.), and visualization was achieved with DAB chromogen. Counterstaining was performed with haematoxylin for 5 sec. The slides were examined under a light microscope (Leica DM2000; Leica Microsystems, Inc.). For NGS, the 5-μm-thick formalin-fixed, paraffin-embedded tissue sections were deparaffinized using alcohol and subsequently hydrated. Sections containing tumour cell-rich regions were microdissected with an ethanol-dipped scalpel. The tissue underwent washing and digestion with phosphate-buffered saline and proteinase K (Qiagen GmbH). DNA extraction was performed using a QIAamp DSP DNA Kit (Qiagen GmbH). Nucleic acid quantification was carried out using a Qubit 4 Fluorometer and fluorescence-based quantitation assays (Thermo Fisher Scientific, Inc.). The quality and integrity of the extracted DNA were assessed using agarose gel electrophoresis and the purity was verified by measuring A260/A280 and A260/A230 ratios with a NanoDrop spectrophotometer (Thermo Fisher Scientific, Inc.). Library preparation utilized the Ion AmpliSeq Library Preparation kit with nucleic acid samples (Thermo Fisher Scientific, Inc.; cat. no. 4475345). DNA sequencing was conducted employing the IonTorrent S5 XL, alongside a control cell line mixture (Horizon Discovery; Revvity Discovery Limited) and a targeted gene panel, the Oncomine Comprehensive Assay Plus (Thermo Fisher Scientific, Inc, cat. no. A48577). The sequencing utilized 200 bp single-end reads. The final library was loaded at a concentration of 50 pM onto the Ion 550 Chip, optimized for the Ion Torrent S5 XL system. This panel facilitates the identification of single nucleotide variants and copy number variants from a pool of

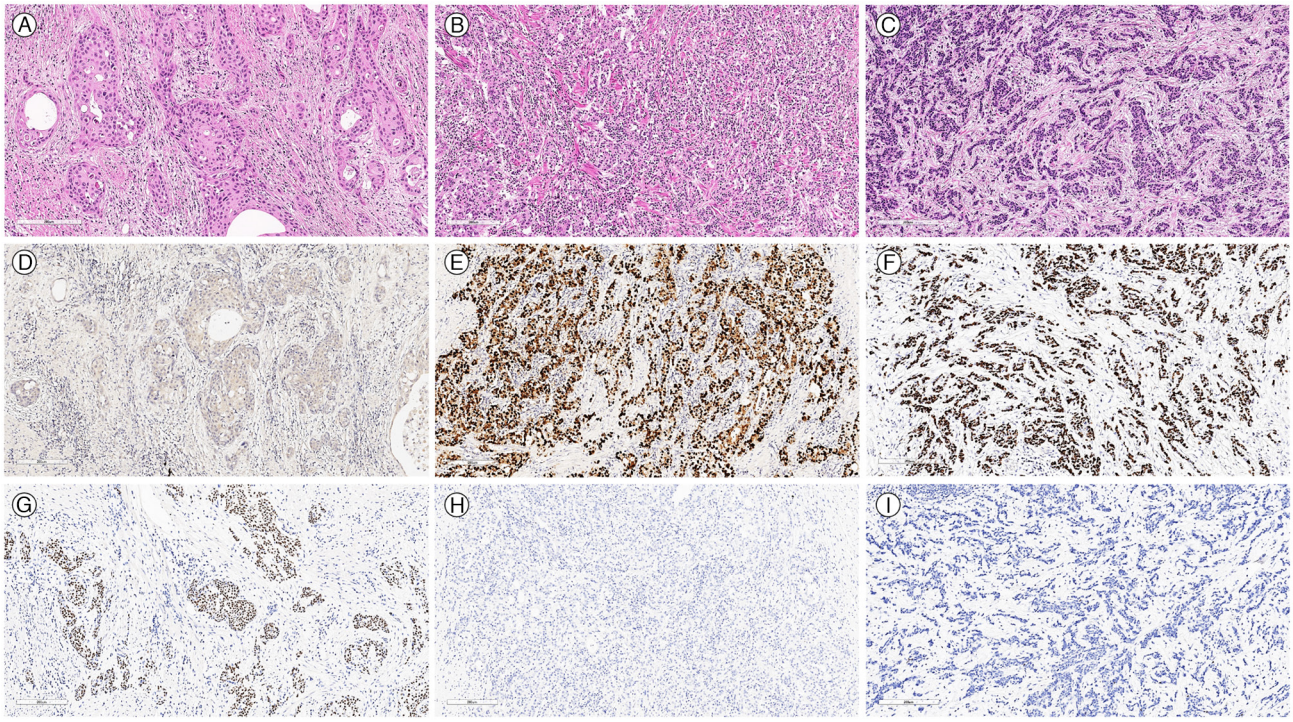


Figure 3. Microscopic images depicting three distinct histological components of the tumour alongside results from EBV *in situ* hybridization and p40 staining. (A) GASC component exhibiting large round to oval nuclei with abundant eosinophilic cytoplasm, intercellular bridges and multifocal glandular formation (H&E; scale bar, 200 μm). (B) GCLS component exhibiting abundant lymphocytic infiltration around undifferentiated carcinoma cell clusters (H&E; scale bar, 200 μm). (C) PDAD component exhibiting hyperchromatic nuclei with mucinous stromal backgrounds with intermittent exhibition of glandular formation (H&E; scale bar, 200 μm). EBV was not detected in the (D) GASC component (scale bar, 200 μm), but was detected in the (E) GCLS (scale bar, 200 μm) and (F) PDAD (scale bar, 200 μm) components. Immunoreactivity for p40 was identified in the (G) GASC component (scale bar, 200 μm), but was negative in the (H) GCLS (scale bar, 200 μm) and (I) PDAD (scale bar, 200 μm) components. GASC, gastric adenosquamous carcinoma; GCLS, gastric carcinoma with lymphoid stroma; PDAD, poorly differentiated adenocarcinoma; EBV, Epstein-Barr virus.

500 gene mutations and 69 gene fusions. For genomic data analysis and variant calling the Ion Reporter software v5.2 was employed (Thermo Fisher Scientific, Inc.).

Representative histological features and images of p40 staining and EBV *in situ* hybridisation for the three tumour components are shown in Fig. 3. The GASC component revealed diffuse immunoreactivity for p40 (Fig. 3G) and p63 as well as focal identification of mucin in the mucicarmine staining (Fig. S1) but was negative for EBV *in situ* hybridisation (Fig. 3D). The GCLS and PDAD components were diffusely positive for EBV *in situ* hybridisation (Fig. 3E and F, respectively) and negative for p40 (Fig. 3H and I, respectively) and p63 staining. All components showed negativity for chromogranin, synaptophysin, PD-1 and HER2 staining, and were positive for MLH1, MSH2 and E-cadherin staining (Fig. S2). The p53 staining showed patchy positivity in all components (Fig. S3). PD-L1 expression (SP142 and SP263) was <1% positive in immune cells and negative in tumour cells in all components. In total, 29 somatic mutations and 14 deletions were identified using the NGS panel; 2 missense mutations and 2 deletions were clinically relevant, whereas the remaining 27 mutations and 12 deletions were variants of uncertain significance. The tumour mutation burden ranged from 5.68 to 6.63, with microsatellite stability in all components. All three histologically distinct components shared common a missense mutation in *PIK3R1* (c.1690A>G, p. Asn564Asp) and homozygous deletions of *ATRX* and *RBM10* (both with copy number 0). The PDAD component exclusively harboured a missense mutation in *TP53*: c.730G>A (p. Gly244Ser). No *PIK3CA* and *ARID1A* mutations, which are prevalent in EBVpGC (15), were identified. The LOF or likely LOF events in *PIK3R1, TP53, ATRX* and *RBM10,* which function as tumour suppressor genes, are classified as oncogenic or likely oncogenic based on the OncoKB database (https://www.oncokb.org/). OncoKB compiles mutation effect information into a database based on various experimental data, functional evidence and *in silico* evidence. According to their standard operating procedure file, a predictive algorithm was utilized, incorporating two programs: SIFT and PolyPhen. The results of NGS analysis for each histologically distinct component are presented in Table I.

Lymph node metastasis was identified in 14 out of 19 lymph nodes (Fig. 4A) and hepatic metastasis was identified via intraoperative liver biopsy (Fig. 4B). The histological features of the metastasis were exclusively of the GCLS component. Accordingly, the TNM stage was determined to be pT4aN3aM1 based on the 8th edition of the American Joint Committee on Cancer Staging System (21). The patient was transferred to another hospital immediately after surgery without chemotherapy or radiotherapy and passed away 6 months later.

Discussion

In the present study a rare case of GC with three distinct histological features, each displaying a different EBV infection state and molecular alteration, yet all sharing common

Table I. Clinically relevant molecular alterations identified by next-generation sequencing.

Gene	Type of genetic alteration	Mutation effect based on *in silico* analysis	Oncogenic effect	HGVS nomenclature	Associated histology in the case
PIK3R1	Missense mutation	LOF	Oncogenic	c.1690A>G (p. Asn564Asp)	GASC, GCLS[a] and PDAD[a]
ATRX	Deletion	Likely LOF	Likely oncogenic	g.76763769_ 77041552del	GASC, GCLS[a] and PDAD[a]
RBM10	Deletion	Likely LOF	Likely oncogenic	g.47006798_ 47046088del	GASC, GCLS[a] and PDAD[a]
TP53	Missense mutation	LOF	Oncogenic	c.730G>A (p. Gly244Ser)	PDAD[a]

[a]Epstein-Barr virus-detected by *in situ* hybridization. HGVS, human genome variation society; LOF, loss-of-function; GASC, gastric adenosquamous carcinoma; GCLS, gastric carcinoma with lymphoid stroma; PDAD, poorly differentiated adenocarcinoma; PIK3R1, phosphoinositide-3-kinase regulatory subunit 1; RBM10, RNA binding motif protein 10.

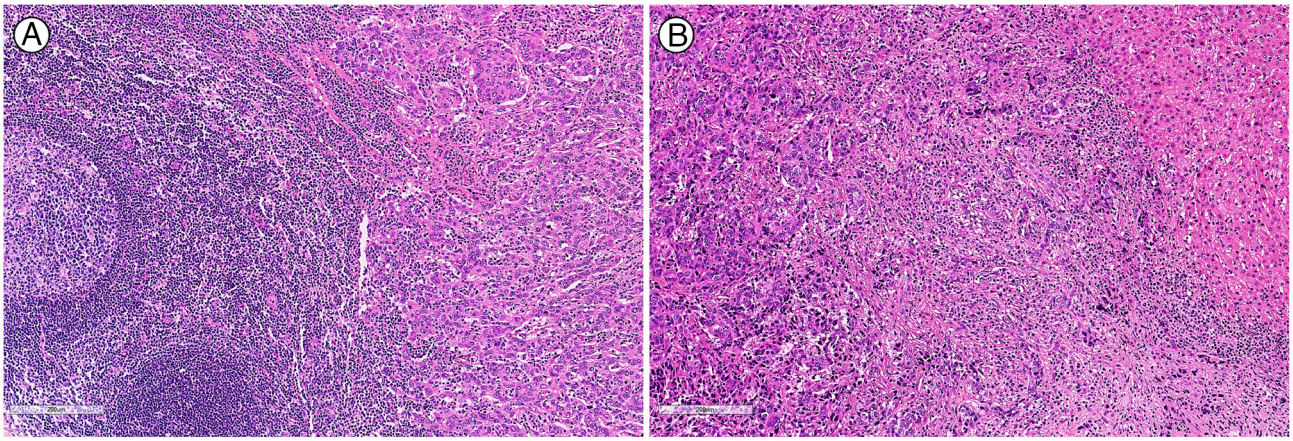


Figure 4. Representative microscopic images of metastatic lesions. (A) lymph node and (B) hepatic parenchyma (H&E; scale bar, 200 μm).

mutations in *PIK3R1*, *ATRX* and *RBM10* was reported. Specifically, the tumour comprised a GASC component without EBV infection, a GCLS component with EBV infection and active *TP53*, and a PDAD component with concurrent EBV infection and *TP53* inactivation. Based on both the molecular and histological findings, the pathogenesis of the present case may be hypothesised as follows: A subset of the tumour, harbouring mutations in *PIK3R1*, *ATRX* and *RBM10*, underwent EBV-driven malignant transformation, manifesting histologically as GCLS and PDAD. Subsequently, the PDAD component of this subset acquired *TP53* inactivation. Evidence from previous studies supports this hypothesis. Knockdown of *ATRX* can induce EBV reactivation (22). Additionally, patients with activated PI3Kδ syndrome due to heterozygous gain-of-function mutations in *PIK3CD* or *PIK3R1* are known to be susceptible to EBV, raising the possibility of EBV susceptibility in patients with LOF mutations in *PIK3R1* (23). Furthermore, *RBM10* has antiviral properties, as upregulation in cells infected with dengue virus inhibits viral replication, while *RBM10* knockdown promotes replication (24). Thus, *RBM10* loss of function may have contributed to the development of EBVpGC.

The pathogenesis of GASC, which constitutes 0.25% of all primary GC cases (20), remains unclear due to its rarity. To date, no studies have investigated the relationship between GASC and *PIK3R1*. EBVpGC is characterised by distinctive genomic alterations, including frequent DNA hypermethylation, *PIK3CA* and *ARID1A* mutations, and an absence of *TP53* mutations (15). EBVpGC is often associated with abundant lymphocytic infiltration surrounding adenocarcinoma clusters, a feature known as GCLS (20). Patients with EBVpGC generally exhibit a longer median survival time compared with those with EBVnGC, with survival times of 8.5 vs. 5.3 years, respectively (17). Although EBVpGC accounts for <10% of all GC cases, it is regarded as a unique entity, distinct from typical gastric adenocarcinoma (15,17). Mutations in *PIK3R1* and *TP53* in EBVpGC were documented in a previous TCGA study. Of the 73 EBVpGC cases, 8 (11%) harboured *PIK3R1* mutations and 11 (15.1%) had *TP53* mutations. By contrast, among the 75 EBVnGC cases, only 1 (1.3%) exhibited a *PIK3R1* mutation, while *TP53* mutations were found in 47 cases (62.7%) (18). These findings suggest that although *PIK3R1* mutations are rare in GC, they may be associated with EBV infection. While most *TP53* mutations are linked to EBVnGC, they can also occur in EBVpGC.

In the present case, the GCLS component displayed typical histological features of EBVpGC with EBV infection. However, unlike prior studies suggesting a favourable prognosis for EBVpGC, the GCLS component resulted in hepatic and lymph node metastases, and the patient passed away within 6 months. This outcome suggests that metastasis may have been driven by the *PIK3R1* mutation, consistent with reports of higher *PIK3R1* expression in advanced stages (III and IV) compared with early stages (I and II) of GC (6).

To date, several cases of mixed EBVpGC with ASC have been reported with histopathological and IHC analyses, but molecular features have not been explored using NGS (25-27). Although a previous study on GC with EBV heterogeneity exists, it differs from the present case in that it did not demonstrate histological heterogeneity or include alterations in *PIK3R1, ATRX* and *RBM10* (28). The underlying cause of EBV infection heterogeneity remains unknown. More comprehensive studies, including multicentre research, are needed to further investigate the implications of EBV infection heterogeneity across diverse histological features.

In conclusion, diverse molecular alterations and EBV infection heterogeneity can be observed in mixed GC across distinct histological components. As these alterations and heterogenous EBV status may influence patient prognosis and treatment strategies, a thorough evaluation of molecular features alongside histological characteristics is crucial.

Acknowledgements

Not applicable.

Funding

This work was supported by a grant from Kyung Hee University in 2024 (grant no. KHU-20241076) and a grant from the Asan Institute for Life Sciences, Asan Medical Center, Seoul, Korea (grant no. 2021IL0040).

Availability of data and materials

The NGS data generated in the present study may be found in the NCBI Sequence Read Archive under accession no. PRJNA1182944 or under the following URL: https://www.ncbi.nlm.nih.gov/sra/PRJNA1182944. All other data generated in the present study may be requested from the corresponding author.

Authors' contributions

Conceptualisation and writing of the original draft were conducted by SUJ. Case selection and investigation of the clinical data was conducted by YK. Review of the H&E slides was conducted by SUJ, EC and SK. NGS analysis and funding acquisition was conducted by SK. Molecular pathology consultation was conducted by JB. Immunohistochemical staining analysis and reviewing and editing the manuscript was conducted by SUJ and SK. SUJ and SK confirm the authenticity of all the raw data. All authors read and approved the final version of the manuscript.

Ethics approval and consent to participate

This retrospective study involves experimental analysis of human tissue specimens collected following surgical procedures. The Institutional Review Board at Ewha Woman's University Mokdong Hospital (Seoul, Republic of Korea) reviewed and approved the study protocol (approval no. 2024-05-004), including a waiver of consent due to the retrospective nature of the study and the patient's death. The study was conducted in accordance with the Declaration of Helsinki.

Patient consent for publication

The Institutional Review Board at Ewha Woman's University Mokdong Hospital (Seoul, Republic of Korea) waived the requirement of patient consent for publication due to the retrospective nature of the study and the patient's death.

Competing interests

The authors declare that they have no competing interests.

Authors' information

Se Un Jeong ORCID, 0000-0001-8399-5792; Euno Choi ORCD, 0000-0002-9284-9276; Yongil Kim ORCID, 0000-0002-4131-364X; Jaeyoung Byeon ORCID, 0009-0002-7316-6549; So-Woon Kim ORCID, 0000-0002-9840-848X.

References

1. Sung H, Ferlay J, Siegel RL, Laversanne M, Soerjomataram I, Jemal A and Bray F: Global cancer statistics 2020: GLOBOCAN estimates of incidence and mortality worldwide for 36 cancers in 185 countries. CA Cancer J Clin 71: 209-249, 2021.
2. Plummer M, Franceschi S, Vignat J, Forman D and de Martel C: Global burden of gastric cancer attributable to helicobacter pylori. Int J Cancer 136: 487-490, 2015.
3. Smyth EC, Nilsson M, Grabsch HI, van Grieken NC and Lordick F: Gastric cancer. Lancet 396: 635-648, 2020.
4. Lordick F, Shitara K and Janjigian YY: New agents on the horizon in gastric cancer. Ann Oncol 28: 1767-1775, 2017.
5. Fattahi S, Amjadi-Moheb F, Tabaripour R, Ashrafi GH and Akhavan-Niaki H: PI3K/AKT/mTOR signaling in gastric cancer: Epigenetics and beyond. Life Sci 262: 118513, 2020.
6. Liu Y, Wang D, Li Z, Li X, Jin M, Jia N, Cui X, Hu G, Tang T and Yu Q: Pan-cancer analysis on the role of PIK3R1 and PIK3R2 in human tumors. Sci Rep 12: 5924, 2022.
7. Xia TF, Chen J, Wu K, Zhang J and Yan Q: Long noncoding RNA NEAT1 promotes the growth of gastric cancer cells by regulating miR-497-5p/PIK3R1 axis. Eur Rev Med Pharmacol Sci 23: 6914-6926, 2019.
8. Li Q, Tian Y, Liang Y and Li C: CircHIPK3/miR-876-5p/PIK3R1 axis regulates regulation proliferation, migration, invasion, and glutaminolysis in gastric cancer cells. Cancer Cell Int 20: 391, 2020.
9. Bartholf DeWitt S, Hoskinson Plumlee S, Brighton HE, Sivaraj D, Martz EJ, Zand M, Kumar V, Sheth MU, Floyd W, Spruance JV, *et al*: Loss of ATRX promotes aggressive features of osteosarcoma with increased NF-κB signaling and integrin binding. JCI Insight 7: e151583, 2022.
10. Aguilera P and López-Contreras AJ: ATRX, a guardian of chromatin. Trends Genet 39: 505-519, 2023.
11. Ge Y, Wei F, Du G, Fei G, Li W, Li X, Chu J and Wei P: The association of sex-biased ATRX mutation in female gastric cancer patients with enhanced immunotherapy-related anticancer immunity. BMC Cancer 21 : 240, 2021.

12. Cao Y, Geng J, Wang X, Meng Q, Xu S, Lang Y, Zhou Y, Qi L, Wang Z and Wei Z: RNA-binding motif protein 10 represses tumor progression through the Wnt/β- catenin pathway in lung adenocarcinoma. Int J Biol Sci 18: 124-139, 2022.
13. Cao Y, Di X, Zhang Q, Li R and Wang K: RBM10 regulates tumor apoptosis, proliferation, and metastasis. Front Oncol 11: 603932, 2021.
14. Sun X, Jia D and Yu Y: Expression pattern, immune signature, and prognostic value of RBM10 in human cancers. Histol Histopathol: 18790, 2024.
15. Saito M and Kono K: Landscape of EBV-positive gastric cancer. Gastric Cancer 24: 983-989, 2021.
16. Yang J, Liu Z, Zeng B, Hu G and Gan R: Epstein-barr virus-associated gastric cancer: A distinct subtype. Cancer Lett 495: 191-199, 2020.
17. Sun K, Jia K, Lv H, Wang SQ, Wu Y, Lei H and Chen X: EBV-positive gastric cancer: Current knowledge and future perspectives. Front Oncol 10: 583463, 2020.
18. He CY, Qiu MZ, Yang XH, Zhou DL, Ma JJ, Long YK, Ye ZL, Xu BH, Zhao Q, Jin Y, *et al*: Classification of gastric cancer by EBV status combined with molecular profiling predicts patient prognosis. Clin Transl Med 10: 353-362, 2020.
19. Cristescu R, Lee J, Nebozhyn M, Kim KM, Ting JC, Wong SS, Liu J, Yue YG, Wang J, Yu K, *et al*: Molecular analysis of gastric cancer identifies subtypes associated with distinct clinical outcomes. Nat Med 21: 449-456, 2015.
20. Carneiro F: Gastric adenocarcinoma. In: WHO Classification of Tumours: Digestive System Tumours. International Agency for Research on Cancer, Lyon, 2019.
21. Amin MB, Edge SB, Greene FL, Byrd DR, Brookland RK, Washington MK, Gershenwald JE, Compton CC, Hess KR, Sullivan DC, *et al*: AJCC cancer staging manual. 8th edition. Springer, New York, NY, 2017.
22. Tsai K, Thikmyanova N, Wojcechowskyj JA, Delecluse HJ and Lieberman PM: EBV tegument protein BNRF1 disrupts DAXX-ATRX to activate viral early gene transcription. PLoS Pathog 7: e1002376, 2011.
23. Carpier JM and Lucas CL: Epstein-barr virus susceptibility in activated PI3Kδ syndrome (APDS) immunodeficiency. Front Immunol 8: 2005, 2018.
24. Pozzi B, Bragado L, Mammi P, Torti MF, Gaioli N, Gebhard LG, García Solá ME, Vaz-Drago R, Iglesias NG and García CC: Dengue virus targets RBM10 deregulating host cell splicing and innate immune response. Nucleic Acids Res 48: 6824-6838, 2020.
25. Cao F, Yan Y, Niu D, Huang X, Jia L, Diao X and Li Z: Epstein-Barr virus-associated gastric adenosquamous carcinoma with concurrent gastric carcinoma with lymphoid stroma: A case report and review of the literature. BMC Gastroenterol 22: 346, 2022.
26. Miyake H, Miyasaka C, Ishida M, Miki H, Inoue K and Tsuta K: Simultaneous gastric adenosquamous carcinoma and gastric carcinoma with lymphoid stroma: A case report. Mol Clin Oncol 11: 77-80, 2019.
27. Kuroda N, Oonishi K, Inoue K, Ohara M, Mizuno K and Lee GH: Lymphoepithelioma-like carcinoma of the stomach associated with adenosquamous carcinoma. Med Mol Morphol 43: 170-173, 2010.
28. Kim HN, Ahn S and Kim KM: Gastric cancer with epstein-barr virus heterogeneity: Evaluation of the frequency, clinicopathologic features, and genomic profiles. Pathol Res Pract 238: 154108, 2022.

Copyright © 2025 Jeong et al. This work is licensed under a Creative Commons Attribution-NonCommercial-NoDerivatives 4.0 International (CC BY-NC-ND 4.0) License.